PNAS RESEARCH ARTICLE | NEUROSCIENCE

Autism-associated *Scn2a* haploinsufficiency disrupts in vivo dendritic signaling and impairs flexible decision-making

Hao Wu[a,b], Luqun Shen[a], Jonathan Indajang[a], Neil K. Savalia[a,b,c], Timothy G. Johnson[a], Jiayin Qu[a], Kevin J. Bender[d], and Alex C. Kwan[a,e,1]

Affiliations are included on p. 11.

Edited by Eunjoon Kim, Korea Advanced Institute of Science and Technology, Daejeon, South Korea; received April 14, 2025; accepted October 16, 2025 by Editorial Board Member Hee-Sup Shin

SCN2A is a high-confidence risk gene for autism spectrum disorder. Loss-of-function mutations in _Scn2a_ reduce dendritic excitability in neocortical pyramidal cells. However, the impact of _Scn2a_ haploinsufficiency on dendritic signaling in vivo, particularly during behavior, is unknown. In this study, we used two-photon microscopy to image dendritic calcium transients in deep layer pyramidal cells in the mouse medial frontal cortex. _Scn2a_$^{+/-}$ mice had diminished coupling between apical and proximal dendritic compartments. Pyramidal tract neurons had abnormal event rates, while intratelencephalic neurons had compartment-specific alterations indicative of diminished dendritic integration. In a matching pennies task, _Scn2a_$^{+/-}$ mice were inflexible in the face of changing competitive pressure. Apical dendritic tuft in intratelencephalic neurons typically encoded reward and strategy, but these task-specific representations were altered in _Scn2a_$^{+/-}$ mice. Collectively, the findings demonstrate that _Scn2a_ haploinsufficiency weakens dendritic integration in vivo and disrupts dendritic encoding of task variables during flexible decision-making.

sodium channel | calcium | dendrite | pyramidal cell | behavioral flexibility

Significance

SCN2A is one of the strongest known genetic risk factors for autism spectrum disorder (ASD). Previous studies using brain slices showed that losing this gene lowers the excitability in dendrites of pyramidal cells in the cortex. However, it was unknown if this occurs in a living brain, especially during behavior. In this study, we used laser-scanning imaging to find that *Scn2a*-deficient mice had reduced integration of dendritic signals. Behaviorally, these mice failed to adjust when playing a matching pennies game with a computer opponent. Moreover, reward and strategy signals in the dendrites were disrupted in *Scn2a*-deficient mice. Overall, our findings offer insight into the neural basis of the cognitive rigidity that characterizes neurodevelopmental disorders.

Autism spectrum disorder (ASD) is a neurodevelopmental condition characterized by deficits in perception, social interaction, and cognition. At the genetic level, studies of rare coding variants have identified numerous high-confidence risk genes for ASD, many of which are involved in signaling and scaffolding in the postsynaptic dendritic compartments (1–3). Although the etiology of ASD remains poorly understood, growing evidence implicates deep layer glutamatergic neurons in the neocortex as key contributors (4). Alterations in excitatory transmission have been observed in many ASD models (5), and the synaptic dysfunctions may be closely tied to abnormalities in dendritic integration (6). Supporting this connection, structural alterations and calcium signaling perturbations to dendrites and dendritic spines have been reported in animal models for ASD (7–9) or autism related disorders such as Fragile X and Angelman syndrome (10, 11). However, uncovering the precise mechanisms by which the genetic perturbations lead to dendritic dysfunctions and ultimately behavioral deficits, remain an ongoing challenge.

Among the most strongly implicated high-confidence risk genes for ASD is *SCN2A* (2, 3). Loss-of-function mutations in *SCN2A* are associated with ASD and intellectual disability, whereas other alterations including gain-of-function mutations are more commonly associated with early onset epilepsy (12–14). *SCN2A* encodes $Na_v1.2$, the type II alpha subunit of a voltage-gated sodium channel found in many cell types and brain regions. In the excitatory pyramidal cells in the neocortex, $Na_v1.2$ is initially localized to the axon initiation segment during early development, but later becomes the dominant isoform expressed in the somatodendritic region in adulthood (15, 16). A function of $Na_v1.2$ is to facilitate membrane excitability. Indeed, in mice with *Scn2a* haploinsufficiency, a disruption of $Na_v1.2$ expression reduces dendrite excitability and impairs synaptic plasticity (15). Specifically, when the cell body is stimulated, calcium influx associated with the backpropagation of action potentials is diminished, reflecting as a decrease in the amplitude in the apical dendritic shaft, and inability to invade into the distal dendritic tuft (15). While these results highlight the importance of *Scn2a* for dendritic function, the studies were performed in acute brain slices. The extent to which these deficits may manifest in vivo and their behavioral relevance are open questions.

Recent advances in two-photon microscopy have provided powerful new approaches for visualizing calcium signals in the dendrites of cortical pyramidal neurons in vivo. The optimization of genetically encoded calcium indicators has yielded reporters with high signal-to-noise ratios, enabling imaging in subcellular compartments of neurons in live mice (17). This improvement has led to exciting discoveries about how synaptic inputs

Preprint server: bioRxiv.

Author contributions: H.W. and A.C.K. designed research; H.W., L.S., J.I., N.K.S., T.G.J., and J.Q. performed research; K.J.B. contributed new reagents/analytic tools; H.W., L.S., and J.I. analyzed data; and H.W. and A.C.K. wrote the paper.

Competing interest statement: A.C.K. has been a scientific advisor or consultant for Boehringer Ingelheim, Eli Lilly, Empyrean Neuroscience, Freedom Biosciences, and Xylo Bio. K.J.B. is an advisor or consultant for Regel Therapeutics, Neurocrine Biosciences, and Emugen Therapeutics. The other authors report no competing interest.

This article is a PNAS Direct Submission. E.K. is a guest editor invited by the Editorial Board.

[1]To whom correspondence may be addressed. Email: alex.kwan@cornell.edu.

This article contains supporting information online at https://www.pnas.org/lookup/suppl/doi:10.1073/pnas.2508836122/-/DCSupplemental.

Published November 20, 2025.

may be propagated and integrated in dendritic compartments. For example, studies have mapped the feature selectivity of inputs impinging at different dendritic locations (18–21), and revealed choice- and reward-related dendritic signals in the sensorimotor cortex during decision-making tasks (22–26). A particularly valuable innovation is the development of multiplane imaging. This technique relies on rapid axial focusing via one of several possible methods such as electrically tunable lens, acousto-optic deflectors, and remote focusing. Multiplane imaging enables near simultaneous recording of fluorescence transients at several depths, which is especially useful for quantifying the coupling between multiple compartments of a neuron including various dendritic branches and the soma in vivo (22, 27, 28).

The goal of this study is to determine the effects of *Scn2a* haploinsufficiency on dendritic calcium signaling in vivo. Performing multiplane imaging using an electrically tunable lens, we visualized calcium transients in the distal apical tuft, apical trunk, and proximal trunk of pyramidal neurons in the mouse medial frontal cortex. We found reduced coupling of dendritic calcium signals in *Scn2a*$^{+/-}$ animals relative to controls. To assess how *Scn2a* haploinsufficiency affects behavior, we developed a competitive decision-making task for head-fixed mice that encourages adaptive strategy switching. *Scn2a*$^{+/-}$ mice were cognitively rigid, failing to adjust to a computer opponent that changes its strategy. During this task, apical dendritic tuft in the frontal cortex normally encoded reward- and strategy-related signals, but these representations were disrupted in *Scn2a*$^{+/-}$ mice. Overall, the results suggest the in vivo dendritic functions in the medial frontal cortex are impaired by *Scn2a* haploinsufficiency, including during flexible decision-making.

Results

Multiplane Imaging of Dendritic Calcium Transients in Frontal Cortical Pyramidal Tract (PT) and Intratelencephalic (IT) Neurons. To study *Scn2a* haploinsufficiency, we compared heterozygous *Scn2a*$^{+/-}$ mice to littermate *Scn2a*$^{+/+}$ controls. Our goal was to characterize dendritic calcium transients in pyramidal cells in the medial frontal cortex (Fig. 1*A*). There are two major subpopulations of pyramidal cells: PT and IT neurons. PT and IT neurons have distinct features; they have different morphological characteristics, physiological properties, and long-range projection targets (29–31). Moreover, PT and IT neurons may have differential contributions to neuropsychiatric conditions and their treatments (32–34). To target a sparse number of PT neurons, we injected a low titer of AAVrg-hSyn-Cre into the ipsilateral pons, and AAV-CAG-Flex-GCaMP6f in the dorsal medial frontal cortex including the anterior cingulate cortex (ACAd) and medial premotor cortex (MOs) (Fig. 1*B*). Fluorescence images of histological coronal sections confirmed a sparse labeling of neurons restricted to the deep layers of the medial frontal cortex, consistent with the expected laminar distribution of PT neurons (Fig. 1*B*).

We imaged spontaneous calcium transients from apical dendritic compartments in the awake, head-fixed mouse. We used two-photon microscopy, with the addition of an electrically tunable lens (ETL) placed above the back aperture of the objective. By applying different electrical currents, the ETL can flex quickly, which allows for a rapid change of the focal plane (35). Prior to time-lapse imaging, we would acquire a z-stack from the pial surface to −500 μm with a step size of 5 μm to identify dendritic segments that belong to the same cell. Then time-lapse imaging commenced, which lasted for 30 min. For each neuron, we would capture fluorescence transients at three focal planes, targeting one depth each for apical tuft (−50 to −150 μm), apical trunk (−250 to −400 μm), and proximal dendrite (<−400 μm) (Fig. 1*D*). The overall frame rate was 7.93 Hz. For analysis, we selected regions of interest (ROIs) corresponding to dendritic segments. We calculated the fractional change in fluorescence $\Delta F/F$ for each ROI.

In control animals, we saw that the dendritic calcium transients between different compartments of a frontal cortical PT neuron were generally synchronized (Fig. 1*E*). That is, whenever there was a calcium transient in one compartment (e.g., an ROI in the plane of apical tuft), we would observe a corresponding calcium transient in other compartments (e.g., ROIs for the apical trunk and the proximal trunk). However, there were also cases when transients were observed in one compartment but not another, such as the leftmost calcium event in the proximal trunk in Fig. 1*E*, which was not detectable in the apical trunk or apical tuft. We noted the signal-to-noise was typically worse in the ROIs at the apical tuft compared to the apical trunk and proximal trunk (*Inset*, Fig. 1*E*), which was expected given the few fluorophores within the small volume of a dendritic segment in the apical tuft. Relatedly, the decay kinetics for the calcium transients was noticeably longer in the apical and proximal trunks, also consistent with these compartments having larger volume and thus needed more time for the clearance of calcium after an influx event (36). Fig. 1*F* shows example dendritic calcium transients imaged from a frontal cortical PT neuron in a *Scn2a*$^{+/-}$ mouse.

Using the same imaging setup, we also characterized the spontaneous calcium transients in the dendrites of frontal cortical IT neurons in the awake, head-fixed mouse. To target a sparse number of IT neurons, we injected a low titer of AAVrg-hSyn-Cre into the contralateral striatum and AAV-CAG-Flex-GCaMP6f in the medial frontal cortex (Fig. 1*C*). Fluorescence images of fixed coronal sections showed sparse labeling of neurons in both superficial and deep layers of the medial frontal cortex, in agreement with the broader distribution of IT neurons (Fig. 1*C*). Because IT neurons tended to have cell bodies that lie more superficially, we targeted the three focal planes slightly differently for apical tuft (−50 to −150 μm), apical trunk (−150 to −350 μm), and proximal dendrite (<−350 μm) (Fig. 1*G*). Fig. 1*H* shows dendritic calcium transients imaged from a frontal cortical IT neuron in a control animal. Fig. 1*I* shows an example from a *Scn2a*$^{+/-}$ mouse.

***Scn2a* Haploinsufficiency Impairs Dendritic Coupling in PT and IT Neurons In Vivo.** Although the calcium transients were mostly synchronized across the different dendritic compartments, we also occasionally observed isolated transients in one compartment only. To quantify the coupling between dendrites, we calculated conditional probabilities. Starting from the $\Delta F/F(t)$ for each ROI, we used the semiautomated OASIS algorithm to infer the underlying electrical events (37). Then, for instance, to determine the amount of transmission from the apical trunk up to the apical tuft, we would consider each event in the apical trunk and tabulate if there was a corresponding event in the apical tuft occurring within ±3 imaging frames. In an example drawn from actual data (Fig. 2*A*), there were 20 events detected in the apical trunk including 2 events that lacked a counterpart in the apical tuft, hence the conditional probability was 0.9. We considered pairwise correlation as another metric that could be used to estimate coupling, but correlation coefficient may be prone to errors because the calcium transients in different dendritic compartments have different decay kinetics.

For PT neurons, we imaged 23 cells in 7 *Scn2a*$^{+/+}$ mice (3 males, 4 females) and 31 cells in 6 *Scn2a*$^{+/-}$ mice (5 males, 1 female) (Dataset S1). We calculated conditional probabilities to estimate the coupling between all imaged ROIs (Fig. 2 *B*–*G*). We note that

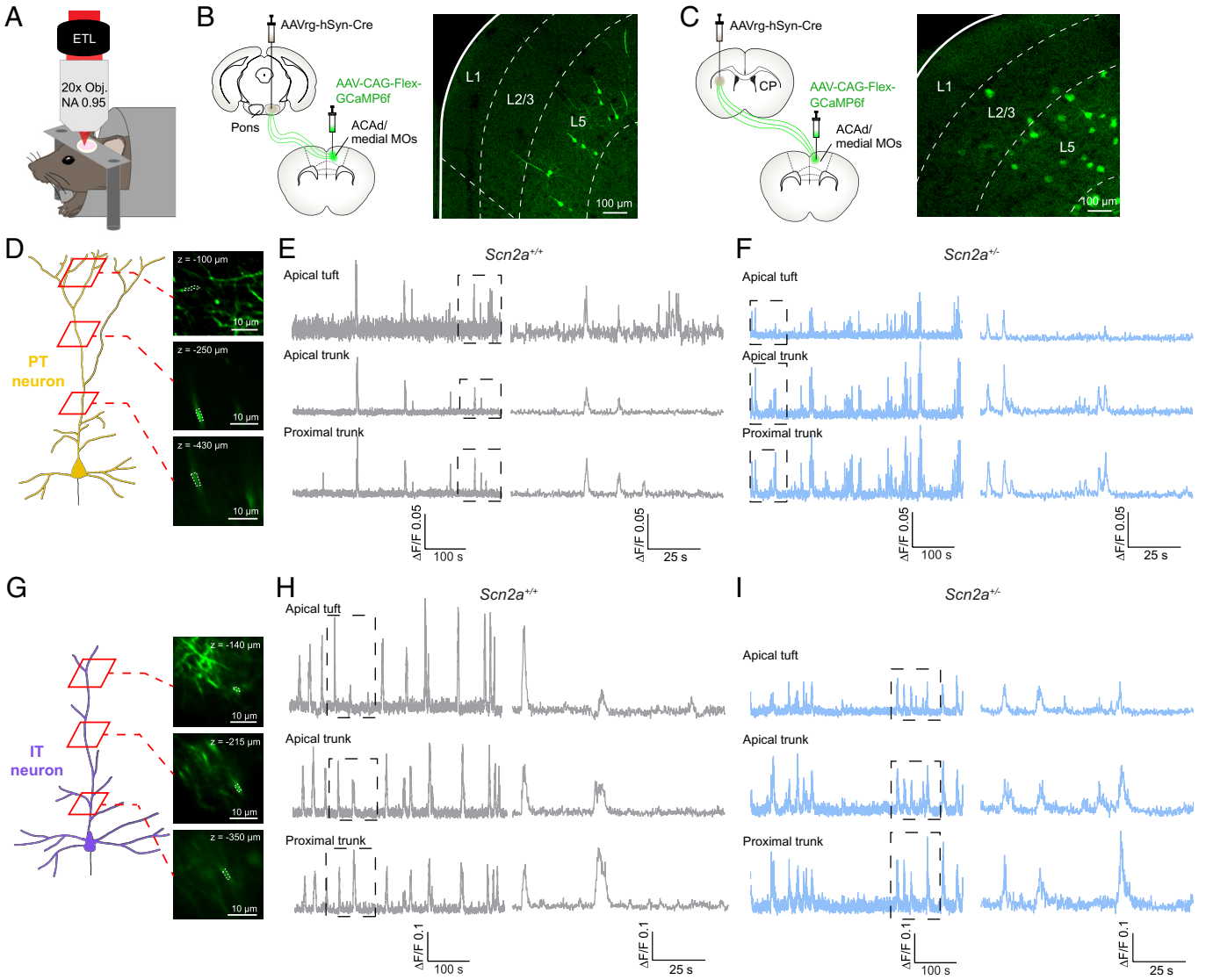

Fig. 1. Imaging calcium transients in the dendritic compartments of single frontal cortical PT or IT neuron. (*A*) The imaging setup involving two-photon imaging of an awake, head-fixed mouse. ETL, electrically tunable lens. (*B*) *Left*, viral strategy to express GCaMP6f in frontal cortical PT neurons. *Right*, fixed coronal section showing GCaMP6f-expressing cells in the medial frontal cortex. White overlay, wireframe from the Allen Mouse Brain Atlas. (*C*) Similar to (*B*) for frontal cortical IT neurons. (*D*) Example two-photon images at different depths corresponding to apical tuft, apical trunk, and proximal trunk of a frontal cortical PT neuron in a *Scn2a*$^{+/+}$ control mouse. Dash lines indicate the region of interest. (*E*) ΔF/F traces from one ROI each from apical tuft, apical trunk, and proximal trunk of a PT neuron in a *Scn2a*$^{+/+}$ control mouse. *Right*, magnified view of the boxed area. (*F*) Similar to (*E*) for a *Scn2a*$^{+/-}$ mouse. (*G–I*) Similar to (*D–F*) for a frontal cortical IT neuron. ACAd, anterior cingulate area dorsal part. MOs, secondary motor cortex. CP, caudate putamen.

some ROIs could come from the same imaging plane (e.g., several ROIs from the same plane for apical tuft of a neuron), therefore for statistical analysis, we used a mixed effects model, which included random effects terms to account for the hierarchical structure of the data where ROIs come from dendrites that may originate from the same mouse (Dataset S2). In the backward direction, the coupling between the proximal trunk and apical tuft was significantly reduced in *Scn2a*$^{+/-}$ mice compared to controls (*Scn2a*$^{+/+}$: 0.75 ± 0.04; *Scn2a*$^{+/-}$: 0.61 ± 0.02; main effect of genotype: P = 0.015, mixed effects model; Fig. 2*B*). The other significant effect associated with *Scn2a* haploinsufficiency was reduced coupling between the apical trunk and the apical tuft (*Scn2a*$^{+/+}$: 0.85 ± 0.02; *Scn2a*$^{+/-}$ mice: 0.77 ± 0.02; main effect of genotype: P = 0.005, mixed effects model; Fig. 2*D*). There was no detected difference in the forward direction for dendritic integration in frontal cortical PT neurons between *Scn2a*$^{+/-}$ and control mice (Fig. 2 *E–G*).

For IT neurons, we imaged 12 cells in 7 *Scn2a*$^{+/+}$ mice (4 males, 3 females) and 13 cells in 5 *Scn2a*$^{+/-}$ mice (1 male, 4 females) (Dataset S1). We found reduced coupling between dendritic compartments in both forward and backward directions (Fig. 2 *H–M*). Similar to PT neurons, we found a significant deficit in the coupling between the proximal trunk and apical tuft in the backward direction (*Scn2a*$^{+/+}$: 0.87 ± 0.02; *Scn2a*$^{+/-}$: 0.71 ± 0.06; main effect of genotype: P = 0.014, mixed effects model; Fig. 2*H*). For the forward direction, propagation of dendritic signal was impaired from the apical tuft to the proximal trunk (*Scn2a*$^{+/+}$: 0.86 ± 0.03; *Scn2a*$^{+/-}$: 0.63 ± 0.06; main effect of genotype: P = 0.002, mixed effects model; Fig. 2*K*), and from the apical trunk to the proximal trunk (*Scn2a*$^{+/+}$: 0.90 ± 0.02; *Scn2a*$^{+/-}$: 0.74 ± 0.04; main effect of genotype: P = 0.001, mixed effects model; Fig. 2*L*). Altogether, these results showed that, in many cases, the coupling between dendritic compartments reduced with the heterozygous loss of $Na_V1.2$. The coupling was most adversely impacted between the

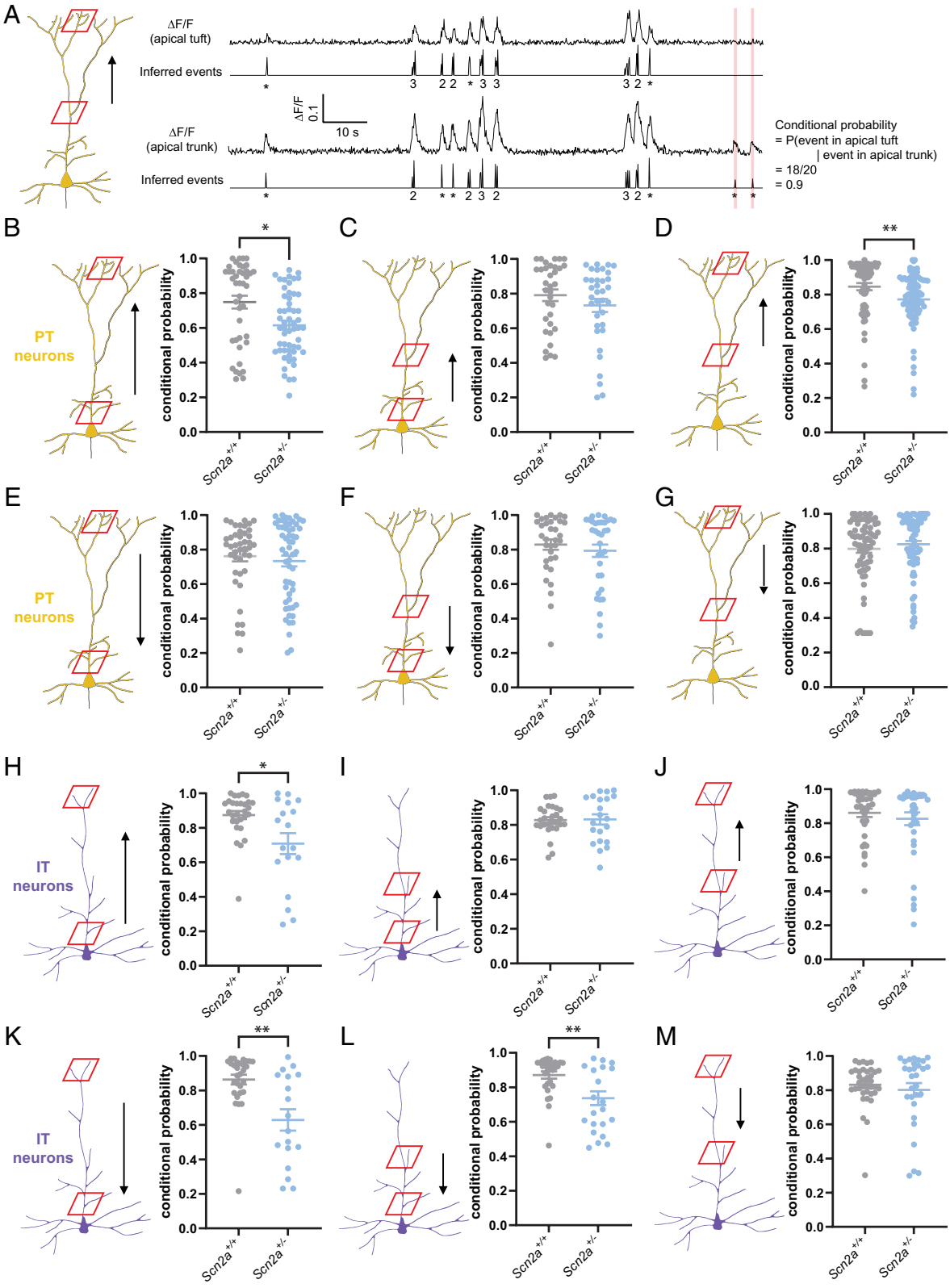

Fig. 2. *Scn2a* haploinsufficiency impairs dendritic coupling in PT and IT neurons in vivo. (*A*) Example ΔF/F traces and the corresponding inferred events from the apical tuft and apical trunk of a PT neuron. The asterisk indicates one inferred event, or else the number indicates the number of inferred events. Red patch, time window centered around an event in apical trunk with no corresponding event in apical tuft. (*B*) Conditional probability of an event in apical tuft given an event in the proximal trunk in PT neurons for $Scn2a^{+/+}$ control animals and $Scn2a^{+/-}$ mice. Each point is a ROI. Mean ± SEM. (*C*) Similar to (*B*) for event in apical trunk given event in proximal trunk. (*D*) Similar to (*B*) for event in apical tuft given event in apical trunk. (*E*) Similar to (*B*) for event in proximal trunk given event in apical tuft. (*F*) Similar to (*B*) for event in proximal trunk given event in apical trunk. (*G*) Similar to (*B*) for event in apical trunk given event in apical tuft. (*H*–*M*) Similar to (*B*–*G*) for IT neurons. *$P < 0.05$. **$P < 0.01$. Linear mixed effects model with fixed effects terms of compartment (proximal trunk, apical trunk, or apical tuft), genotype ($Scn2a^{+/+}$ or $Scn2a^{+/-}$), cell type (PT or IT), and all interactions, with ROI per dendrite per mouse modeled as nested random intercepts. See Dataset S2.

apical tuft and the proximal trunk, which span the greatest distance across the PT and IT neurons in our analysis.

From the events inferred from $\Delta F/F$ for each ROI, we could determine the rate of the dendritic calcium transients. We found that there were compartment and cell type specific differences in the dendritic calcium transients (genotype × compartment interaction: $P = 0.021$, compartment × cell type interaction: $P = 0.0003$, mixed effects model; Dataset S2). For PT neurons, their dendrites were overall more active in *Scn2a*$^{+/-}$ mice than control animals, irrespective of the dendritic compartment ($P = 5 \times 10^{-7}$, Bonferroni post hoc test; *SI Appendix*, Fig. S1*A*). For frontal cortical IT neurons, there was no main difference across genotypes ($P = 0.8$, Bonferroni post hoc test), but the frequency of calcium events varied across the dendritic compartments (*SI Appendix*, Fig. S1*D*). Namely, we found that in *Scn2a*$^{+/-}$ animals, the calcium event rate was higher in the apical tuft and apical trunk than the proximal trunk (apical tuft vs. proximal trunk: $P = 0.033$, apical trunk vs. proximal trunk: $P = 0.035$, apical tuft vs. apical trunk: $P = 0.6$, Bonferroni post hoc test). The reduced event rate in the proximal trunk is consistent with the deficient forward transmission in IT neurons in *Scn2a*$^{+/-}$ animals (Fig. 2 *K* and *L*). In addition to event rate, the partial loss of *Scn2a* also affected the amplitude and decay time of the fluorescence transients (*SI Appendix*, Fig. S1 *B*, *C*, *E*, and *F* and Dataset S2). This analysis demonstrates an aberrant elevation in dendritic calcium events specifically in the PT neuron subpopulation because of *Scn2a* haploinsufficiency, which may compensate for the deficient coupling across dendritic compartments.

***Scn2a*-Haploinsufficient Mice Were Inflexible against Changing Behavioral Strategies.** So far, our results have revealed how *Scn2a* haploinsufficiency affects in vivo spontaneous activity in the dendrites, but we also want to know the potential alterations during behavior. The dorsal medial frontal cortex in rodents is involved in adaptive decisions involving behavioral flexibility (38). We therefore tested the animals on various decision-making paradigms. Initially, we trained *Scn2a*$^{+/-}$ mice to perform a probabilistic reward reversal task, but observed no alteration in performance compared to control animals (39). Next, we trained *Scn2a*$^{+/-}$ mice to play a standard version of the matching pennies game that we previously adapted for head-fixed mice (40, 41). Matching pennies is a classic two-playing competitive game (42). In this standard version, the two players are the mouse and a computer, with the computer programmed to always play with the same strategy. We again found that *Scn2a*$^{+/-}$ mice performed to a level that was not distinguishable from control animals (*SI Appendix*, Fig. S2). We surmised that these tasks may not sufficiently assess flexible behavior, because the animal can rely on the same behavioral strategy for the entire task. For the probabilistic reward reversal, mice can excel by using a finite-state approach, e.g., choosing the high-reward option repeatedly, until encountering a few reward omissions, then switching to the other option (43, 44). For matching pennies, since the computer always used the same strategy, animals could counter by employing a strategy of randomly choosing between the two options (40, 45). Instead, ASD-related cognitive deficits may be accentuated in tasks that encourage flexibility in behavioral strategies.

We therefore designed a task, still based on matching pennies, but the animal faces a computer opponent that can switch strategies. In other words, the rules of the game—payoff matrix and trial timing—always remain the same, but the innovation is that we programmed three different strategies for the computer opponent. Briefly, a head-fixed mouse would play against a computer opponent (Fig. 3*A*). Each trial, the mouse would indicate a choice between the left and right options using a directional tongue lick. The computer would also choose one of the options. The payoff matrix is shown in Fig. 3*B*. If the mouse and computer chose the same option (i.e., both picked left or both picked right), then the mouse would receive a reward of ~4 μL of water. If the mouse and computer chose different options (i.e., mouse picked left and computer picked right, or vice versa), then the mouse would have no reward. A trial began when a motor actuator advanced the two lick spouts to just in front of the mouse's head (Fig. 3*C*). Then a sound cue was played, which was followed by a 2-s response window. Depending on the mouse's choice (first lick during the response window) and the payoff matrix, water would be delivered immediately if the mouse won the trial. Subsequently, the motor actuator would retract and there was a random intertrial interval between each trial. The computer can play with one of three possible strategies. The "predictive" strategy is a strong player that would play by predicting the mouse's next choice based on the history of past choices and outcomes in that session (same as the strategy used in ref. 40, algorithm 2 in ref. 46, and competitor 1 in ref. 45). The "WSLS" strategy stands for win-stay, lose-switch, where the computer would pick the same option if it won the last trial or switch options if it lost the last trial. Finally, the "alternate" strategy is when the computer would choose left, right, left, right, and so on, regardless of the mouse's previous choices and outcomes.

We trained *Scn2a*$^{+/-}$ and control mice to play the matching pennies game against a computer opponent using the predictive strategy until the animals became proficient (>35% reward rate for 3 consecutive days). Then we tested them on the matching pennies game with the exact same rules, but now against a computer opponent that switched its strategy every 90 to 110 trials during a session. Fig. 3*D* shows a control mouse playing matching pennies when the computer opponent started with the predictive strategy, switched to WSLS, and then toggled for the remainder of the session. We characterized the animals' performance in 130 sessions from 38 *Scn2a*$^{+/+}$ mice (16 males, 22 females) and 108 sessions from 25 *Scn2a*$^{+/-}$ mice (15 males, 10 females). On a per-animal basis, the control animals had a probability of switching their option at 36.5 ± 1.5% during predictive blocks and 39.5 ± 2.0% during WSLS blocks (Fig. 3*E*). The *Scn2a*$^{+/-}$ animals had a probability of switching their option at 35.6 ± 1.2% during predictive blocks and 35.0 ± 1.1% during WSLS blocks (Fig. 3*F*). Although the differences in performance on aggregate was obscured by variability across individuals (Fig. 3 *G* and *H*), we can analyze how each animal adapted by calculating its switching probability during predictive block relative to during WSLS block (*Scn2a*$^{+/+}$: −2.9 ± 0.9%; *Scn2a*$^{+/-}$: 0.6 ± 0.9%; Fig. 3*I* and (*SI Appendix*, Fig. S3 *A*–*F*). To determine statistical significance, we analyzed per-session data using a mixed effects model that included fixed effects terms for genotype, computer strategy, and their interaction, as well as random effects terms to account for the hierarchical structure of the data where sessions come from the same mouse. We detected a significant impairment for the *Scn2a*$^{+/-}$ mice to adjust to the changing strategy relative to control animals ($P = 0.033$, genotype × strategy interaction; Dataset S3). In agreement, logistic regression analysis showed that control animals had a significant tendency to switch following a rewarded choice during WSLS blocks, but not *Scn2a*$^{+/-}$ mice (*SI Appendix*, Fig. S4). This is a beneficial adaptation for the control animals, because a player should switch more during WSLS. In fact, to maximize reward rate, an optimal player should be switching half the time against the predictive strategy but switch all the time against the WSLS strategy.

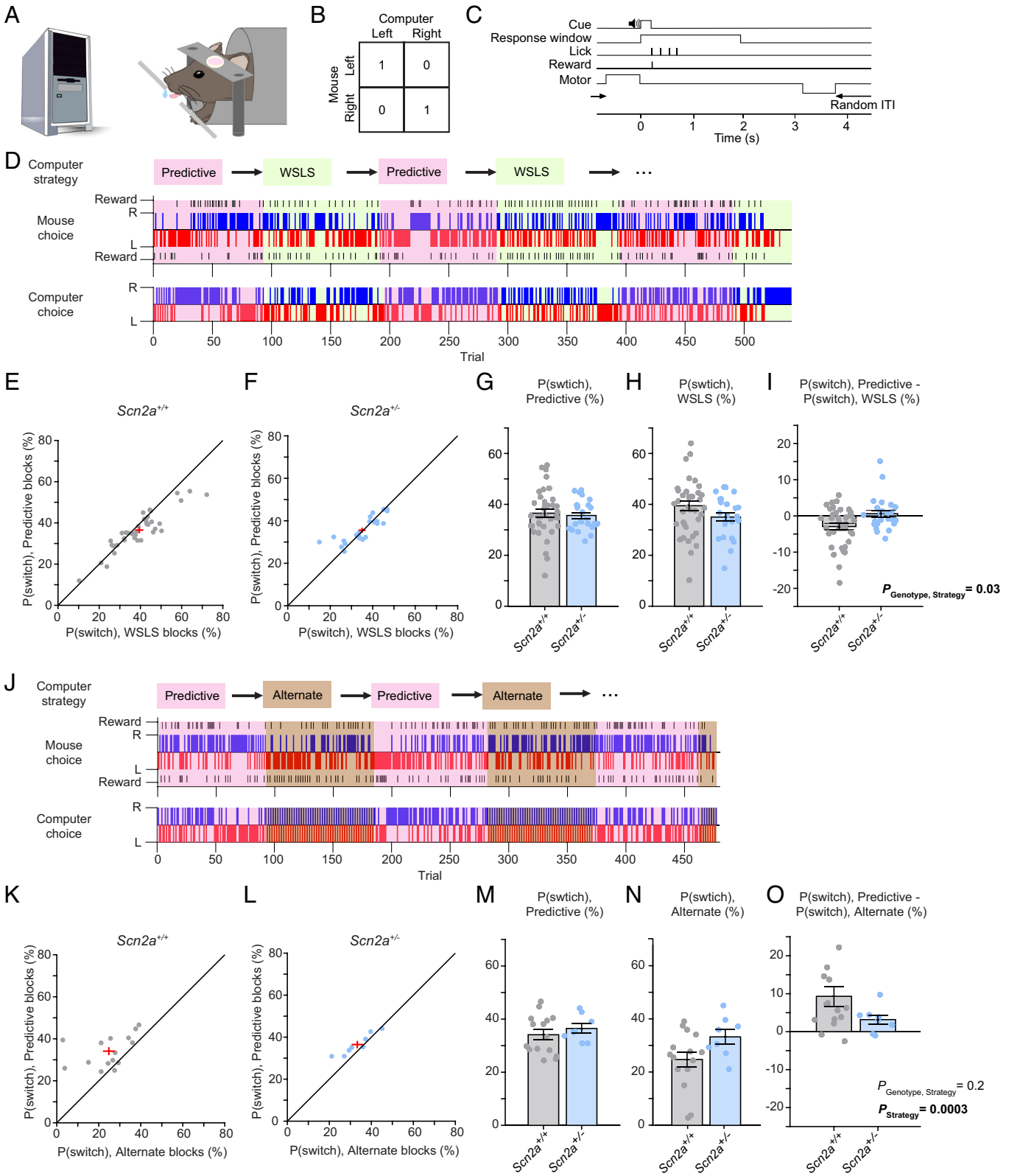

Fig. 3. *Scn2a*-haploinsufficient mice were inflexible against changing behavioral strategies. (*A*) Behavioral setup. (*B*) The payoff matrix of the matching pennies game. 1 denotes a reward for the mouse, and 0 denotes no reward. (*C*) The trial timing. (*D*) An example session when a mouse played matching pennies with a computer opponent that changed strategies between predictive (pink shading) and WSLS (green shading). *Top* row, the strategy used by the computer. *Middle* row, the mouse's choices and outcomes. *Bottom* row: computer's choices. Black line, reward. (*E*) The switch probability during predictive and WSLS trials for $Scn2a^{+/+}$ control mice. Each point represents the mean value of a mouse. Red crosshair, Mean ± SEM. (*F*) Similar to (*E*) for $Scn2a^{+/-}$ mice. (*G*) Bar plot of the switch probability when the computer used predictive strategy. Each point represents the mean value of a mouse. Mean ± SEM. (*H*) Similar to (*G*) when the computer used WSLS strategy. (*I*) Bar plot of the switch probability difference between predictive trials and WSLS trials. Each point represents the mean value of a mouse. Mean ± SEM. (*J*–*O*) Similar to (*D*–*I*) for a computer opponent that changed strategies between predictive (pink shading) and alternate (brown shading). Note that for panel *O*, there is an outlier for $Scn2a^{+/+}$ mice at 36.6 not included in the plot.

We also trained animals playing matching pennies when the computer opponent was swapping between the predictive and alternate strategies (Fig. 3*J*). We had a smaller dataset, which included 60 sessions from 15 *Scn2a*$^{+/+}$ mice (7 males, 8 females) and 38 sessions from 8 *Scn2a*$^{+/-}$ mice (4 males, 4 females). The control animals had a probability of switching their option at 34.1 ± 1.9% during predictive blocks and 24.8 ± 2.8% during alternate blocks (Fig. 3*K*). The *Scn2a*$^{+/-}$ animals had a probability of switching their option at 36.5 ± 1.8% during predictive blocks and 33.3 ± 2.7% during alternate blocks (Fig. 3*L*). We quantified how each animal adapts by calculating its switching probability during the predictive blocks relative to during the alternate blocks, we did not detect a significant difference between the genotype (*Scn2a*$^{+/+}$: 9.3 ± 2.6%; *Scn2a*$^{+/-}$: 3.2 ± 1.2%; Fig. 3 *M–O* and *SI Appendix*, Fig. S3 *G–L*). Applying a mixed effects model for statistical analysis, we did not detect a difference between *Scn2a*$^{+/-}$ mice and control animals (P = 0.18, genotype x strategy interaction), with both genotypes adjusting to the computer opponent's alternate strategy (P = 0.0003, main effect of strategy; Dataset S3). The adjustment was a shift to perseverative choice behavior, which we speculate was due to their desire to minimize effort, which may relate to a previous study reporting that when the computer's choice is not contingent on the animal's decision, the animal would stick to the same option repeatedly (46).

Altogether, these results demonstrate that control mice can adjust their behavior while playing matching pennies with computer opponents employing different strategies. Notably, they switched more frequently against the WSLS strategy but less against the alternate strategy, showing behavioral flexibility in both directions from their likely overtrained responses to the predictive strategy. *Scn2a*$^{+/-}$ mice, by contrast, showed significantly reduced adaptability, and did not deviate from their initial trained behavior.

Trial-Modulated Signals in the Apical Dendritic Tuft of PT and IT Neurons. We observed reduced dendritic coupling during spontaneous activity in both PT and IT neurons in *Scn2a*$^{+/-}$ mice; however, it is still unclear whether there may be potential deficit in dendritic signaling during behavior. We therefore hypothesize that dendritic dysfunction in the medial frontal cortex may relate to the inflexibility in decision-making in *Scn2a*$^{+/-}$ mice. To investigate this possibility, we imaged dendritic calcium signals from PT and IT neurons while the mouse was playing the matching pennies game against a computer opponent switching between the predictive and WSLS strategies (Fig. 4*A*). The dual viral injection strategy used for Fig. 1 enabled imaging of the same dendritic tree from single neurons; however, the sparse labeling approach had a low success rate, often leading to zero or dense labeling. Here, to increase the yield because we also needed to invest time to train animals, we leveraged the Cre-driver lines *Fezf2-2A-CreER* to target cortical PT neurons and *PlexinD1-2A-CreER* to target cortical IT neurons (47). We injected AAV-CAG-Flex-GCaMP6f into the ACAd and medial MOs portion of the medial frontal cortex of *Fezf2-CreER*$^{+/-}$*::Scn2a*$^{+/-}$ mice, with *Fezf2-CreER*$^{+/-}$*::Scn2a*$^{+/+}$ as controls, or *PlexinD1-CreER*$^{+/-}$*::Scn2a*$^{+/-}$ mice, with *PlexinD1-CreER*$^{+/-}$*::Scn2a*$^{+/+}$ as controls (Fig. 4*B*). We administered tamoxifen to induce Cre-mediated expression of GCaMP6f. We focused on imaging dendritic segments from the apical tuft located 50 to 100 µm below the pial surface (Fig. 4 *C* and *D*).

We aligned fluorescence transients to the time of the sound cue onset, which revealed trial-modulated signals in the apical dendritic tuft in PT and IT neurons (Fig. 4 *E–J*). Mostly, fluorescence transients occurred at approximately −1, 0, or 3 s relative to cue onset, corresponding to the times during a trial when the motorized actuator was advancing the lick spouts, the animal was making a lick choice and receiving the outcome, or when the motorized actuator was retracting the lick spouts. Fig. 4*F* shows two ROIs from PT neurons in a control mouse that had trial-modulated activity, although no differential modulation by choice or outcome. By contrast, some apical dendritic tufts of PT neurons in *Fezf2-CreER*$^{+/-}$*::Scn2a*$^{+/-}$ mice exhibited outcome selectivity, for example here both ROIs 1 and 2 larger $\Delta F/F$ in rewarded trials relative to unrewarded trials (Fig. 4*G*). Fig. 4*I* shows example ROIs from IT neurons in a control animal. Fluorescence increased in ROI 1 when the animal chose left and received a reward, relative to all other conditions. This indicates a preference for the choice × outcome interaction, specifically for left and reward. ROI 2 exhibited higher fluorescence when there was a reward together with either a left or right choice, which reflected an outcome-related signal. Fig. 4*J* shows two example ROIs from a control *PlexinD1-CreER*$^{+/-}$*::Scn2a*$^{+/-}$mouse. These were trial-modulated signals but not selective for specific choice or outcome.

In total, for PT neurons, we imaged 129 ROIs during 5 sessions from 2 *Fezf2-CreER*$^{+/-}$*::Scn2a*$^{+/+}$ mice (2 males) and 861 ROIs during 30 sessions from 8 *Fezf2-CreER*$^{+/-}$*::Scn2a*$^{+/-}$ mice (5 males, 3 females) (Dataset S1). To quantify the fraction of ROIs that exhibited trial-modulated signals, we determined whether there was a significant difference in $\Delta F/F$ between the cue period (t = −0.5 to 0.5 s) and baseline (t = −2 to −1 s) or between the outcome period (t = 1 to 2 s) and baseline (t = −2 to −1 s). The majority of ROIs exhibited trial-modulated signals, and the proportions were not different with the partial loss of *Scn2a* than controls for cue period (t = −0.5 to 0.5 s; control: 53.4 ± 9.4%; *Fezf2-CreER*$^{+/-}$*::Scn2a*$^{+/-}$: 66.7 ± 4.8%; P = 0.2, Wilcoxon rank sum test) or outcome period (t = 1 to 2 s; control: 61.2 ± 3.7%; *Fezf2-CreER*$^{+/-}$*::Scn2a*$^{+/-}$: 49.1 ± 4.6%; P = 0.3, Wilcoxon rank sum test; Fig. 4*K*). For IT neurons, we imaged 357 ROIs from IT neurons during 17 sessions from 4 *PlexinD1-CreER*$^{+/-}$*::Scn2a*$^{+/+}$ mice (2 males, 2 females) and 271 ROIs during 14 sessions from 4 *PlexinD1-CreER*$^{+/-}$*::Scn2a*$^{+/-}$ mice (4 males). Similarly, most ROIs had trial-modulated signals, with the proportions not different across genotype for cue period (control: 74.3 ± 4.3%; *PlexinD1-CreER*$^{+/-}$*::Scn2a*$^{+/-}$: 60.2 ± 7.5%; P = 0.1, Wilcoxon rank sum test) or outcome period (control: 55.0 ± 6.2%; *PlexinD1-CreER*$^{+/-}$*::Scn2a*$^{+/-}$: 47.8 ± 7.7%; P = 0.6, Wilcoxon rank sum test; Fig. 4*L*). This analysis indicates that most dendritic segments of frontal cortical PT and IT neurons had trial-modulated calcium transients while the mice were engaged in the matching pennies task.

Reward- and Strategy-Related Signals Were Altered in the Dendrites of *Scn2a*-Haploinsufficient Mice. To characterize the factors that account for the calcium signals in the apical dendritic tufts of PT and IT neurons during matching pennies, we used multiple linear regression. For each ROI, we fitted a regression model to determine how the fluorescence transient $\Delta F/F(t)$ relates to the choices (left or right), outcomes (reward or no reward), and their interactions for the current and past trials, as well as strategies (predictive or WSLS) and their interactions (Fig. 5*A*). For PT neurons, the regression analysis showed that fluorescence transients did not significantly encode any of the task variables tested in control animals (Fig. 5 *B* and *C*). Surprisingly, with the partial loss of *Scn2a* in the in *Fezf2-CreER*$^{+/-}$*::Scn2a*$^{+/-}$ mice, we observed that some dendritic calcium signals began to display preference for specific outcome of the current trial and the strategy (Fig. 5*D*). By contrast, when we applied the same multiple linear regression for ROIs from IT neurons, the analysis revealed that ~7% of the ROIs were

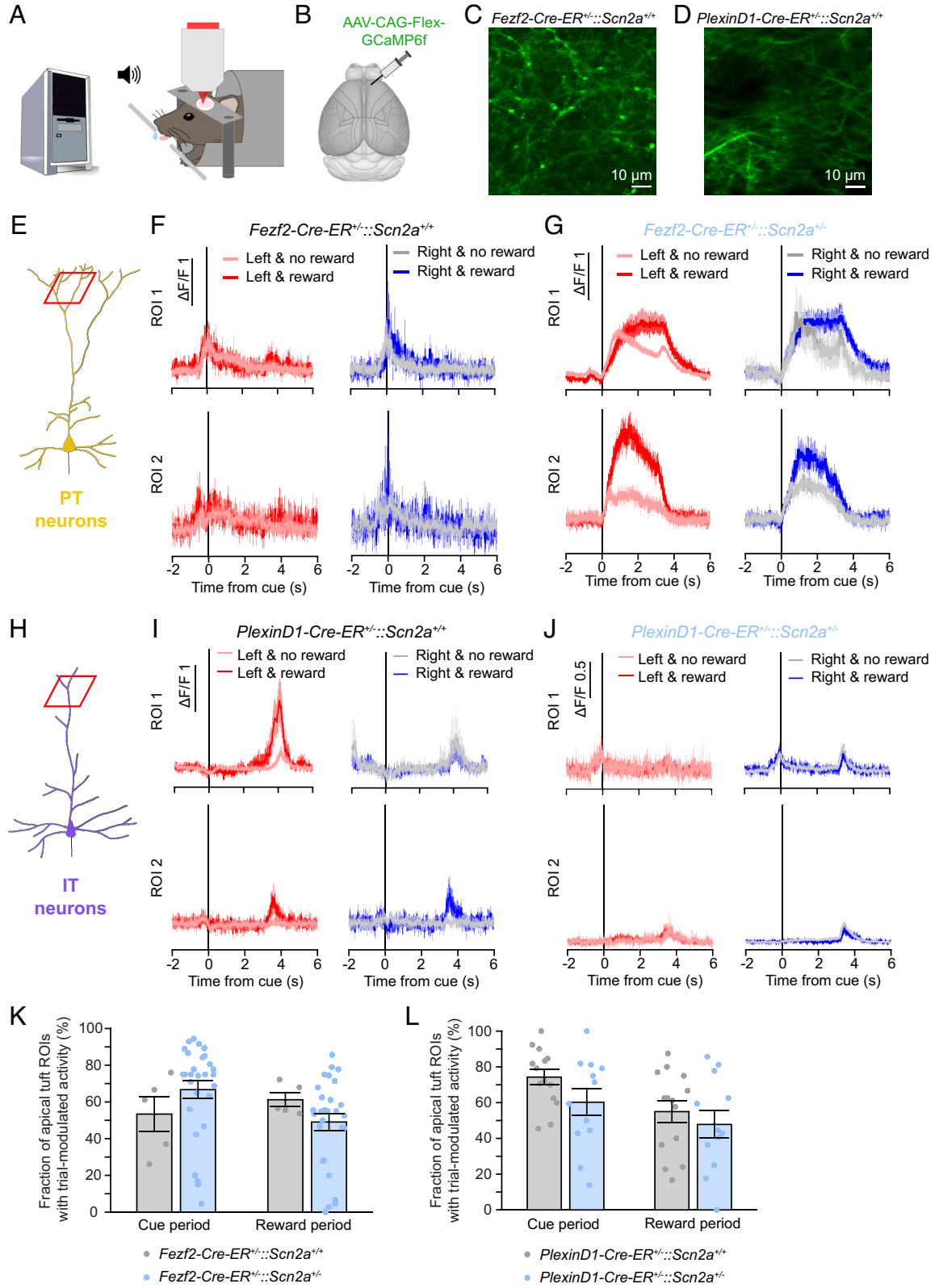

Fig. 4. Trial-modulated activity in the apical dendritic tuft of PT and IT neurons. (*A*) Experimental setup. (*B*) Viral strategy to express GCaMP6f in PT or IT neurons in the frontal cortex in a mouse. (*C*) Example two-photon image of GCaMP6f-expressing apical tuft dendrites in a *Fezf2-CreER*$^{+/-}$*::Scn2a*$^{+/+}$ mouse. (*D*) Example two-photon image of GCaMP6f-expressing apical tuft dendrites in a *PlexinD1-CreER*$^{+/-}$*::Scn2a*$^{+/+}$ mouse. (*E*) Diagram of ROI selection in apical tufts in PT neurons. (*F*) Trial-averaged ΔF/F from trials with different choices and outcomes for two example ROIs in a *Fezf2-CreER*$^{+/-}$*::Scn2a*$^{+/+}$ control mouse. (*G*) Similar to (*F*) in a *Fzef2-CreER*$^{+/-}$*::Scn2a*$^{+/-}$ mouse. (*H*) Diagram of ROI selection in apical tufts in IT neurons. (*I*) Trial-averaged ΔF/F from trials with different choices and outcomes for two example ROIs in a *PlexinD1-CreER*$^{+/-}$*::Scn2a*$^{+/+}$ control mouse. (*J*) Similar to (*I*) in a *PlexinD1-CreER*$^{+/-}$*::Scn2a*$^{+/-}$ mouse. (*K*) The fraction of ROIs in PT neurons with trial-modulated activity, defined as significant difference in ΔF/F during cue (t = −0.5 to 0.5 s) or outcome period (t = 1 to 2 s), relative to baseline (t = −2 to −1 s). (*L*) Similar to (*K*) in IT neurons.

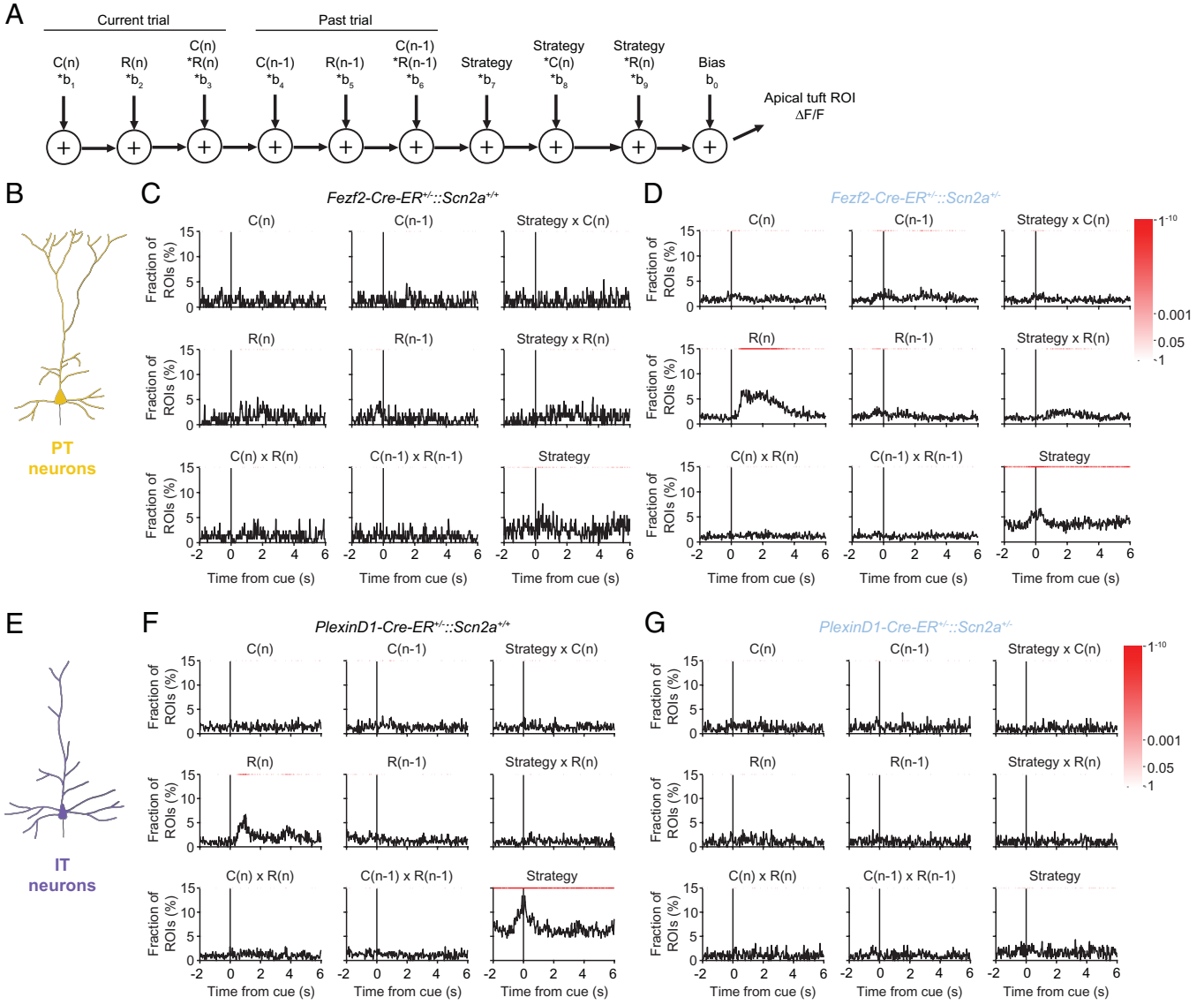

Fig. 5. Reward- and strategy-related signals in the dendrites were altered in *Scn2a*-haploinsufficient mice. (*A*) The multiple linear regression model used to fit the ΔF/F of a ROI from the apical tuft of PT and IT neurons. (*B*) Diagram of a PT neuron. (*C*) Fraction of ROIs in *Fezf2-CreER*$^{+/-}$*::Scn2a*$^{+/+}$ control animals with statistically significant ($P < 0.01$) regression coefficients for the various predictor variables. Red shading indicates *P*-value calculated based on the binomial test. (*D*) Similar to (*C*) in *Fezf2-CreER*$^{+/-}$*::Scn2a*$^{+/-}$ mice. (*E*) Diagram of an IT neuron. (*F*) Similar to (*C*) in *PlexinD1-CreER*$^{+/-}$*::Scn2a*$^{+/+}$ mice. (*G*) Similar to (*C*) in *PlexinD1-CreER*$^{+/-}$*::Scn2a*$^{+/-}$ mice.

modulated by the outcome of the current trial in control animals (Fig. 5 *E* and *F*). The strategy of the computer opponent was robustly represented, especially around the time of cue when decisions were made. These outcome- and strategy-selective signals were absent in apical dendritic tufts in the *PlexinD1-CreER*$^{+/-}$*::Scn2a*$^{+/-}$mice (Fig. 5*G*). To summarize, unlike earlier studies that reported reward-related firing changes persisting for a few trials in a substantial portion of frontal cortical neurons (38, 48–52), here we observed that outcome- and strategy-related signals were more transient and only present in a small subset of apical dendritic tufts. The fraction of ROIs that has task-related representations was low, which could be due to the low signal-to-noise ratio in our dendritic imaging conditions, or due to substantial contributions from uninstructed movements not associated with the task (53, 54) or arousal-related factors (55), which were not captured by our model. The overall explained variance captured by the regression model is low, which is a limitation to consider when interpreting the results. Despite this caveat, our results suggest that *Scn2a* haploinsufficiency alters the typical pattern of dendritic signals in the apical tuft of frontal cortical PT and IT neurons during decision-making.

Discussion

The results in this study support three main conclusions. One, *Scn2a* haploinsufficiency impairs the coupling between apical and proximal dendritic compartments in PT and IT pyramidal neurons in the medial frontal cortex. Two, *Scn2a*$^{+/-}$ mice exhibited cognitive rigidity, where they were unable to adapt to the changing strategy of a computer opponent in a matching pennies game. Three, reward- and strategy-related signals in the dendrites of frontal cortical PT and IT neurons were disrupted in *Scn2a*-haploinsufficient mice during decision-making.

Numerous studies have investigated the coupling between dendritic and somatic compartments in cortical pyramidal neurons in vivo. In anesthetized animals, layer 5 pyramidal neurons in the barrel cortex exhibit varied coupling between the apical dendrites and proximal soma (56). Specifically, large calcium signals in the apical dendrites are associated with burst firing in the soma. These correlated events may be elicited by whisker stimulation or by backpropagating action potentials. The fluorescence transients detected in our study are likely associated with these burst firing

events rather than single action potentials, as indicated by the relatively low rate of calcium events and the sensitivity of the genetically encoded calcium indicator under our imaging conditions (36). Our observation of high level of dendritic coupling in control animals also aligns with other prior works. A previous study suggests that layer 5 pyramidal neurons in the anterior cingulate cortex may exhibit more reliable signal propagations between soma and dendrite compared to those in the sensory cortex (57). In the awake animal, increased background excitatory activity would elevate dendritic excitability, which should strengthen the coupling between somatic, proximal, and apical compartments (58, 59). Indeed, other recent studies in awake mice reported a close correspondence of calcium transients between distal apical dendrites and locations proximal to the cell body (22, 27, 60). Our results are in agreement with these earlier studies to show a high degree of dendritic coupling in the medial frontal cortex of awake animals.

Scn2a encodes the voltage-gated sodium channel $Na_v1.2$, which localizes to dendrites of neocortical pyramidal cells after the first postnatal week, and is expected to support dendritic excitability. Indeed, in brain slices, one could evoke dendritic calcium signal via backpropagation by stimulating the cell body, and this signal was reduced with the heterozygous loss of $Na_v1.2$ (15). Our study adds to this finding by showing the impact of *Scn2a* haploinsufficiency on the transmission of signals in dendrites in vivo in awake animals. We further found cell-type specific differences. PT neurons had impaired coupling affecting transmission from the proximal and apical trunk up to the apical tuft in *Scn2a*$^{+/-}$ animals. Accompanying this decoupling in the backward direction is an aberrant elevation in the number of calcium events in the apical tuft. By contrast, IT neurons had diminished dendritic signaling in both the forward and backward directions, and its calcium event rates were not changed by *Scn2a* haploinsufficiency. Though we note that a caveat of the current study is that we are estimating directional effects based on conditional probability, but have not directly measured the propagation of calcium signals which would require much higher temporal resolution for the imaging. The aberrant calcium event rates may relate to the paradoxical increase in action potential excitability seen in cortical pyramidal neurons following the deletion of *Scn2a* (61, 62). For future studies, knowing the distribution of $Na_v1.2$ in the dendritic tree of individual frontal cortical PT and IT neurons would allow us to further interpret and model the current data.

Our motivation for selecting a decision-making task was based on two main considerations. First, individuals with ASD exhibit core deficits in social interaction and impairments in decision-making, particularly in computations related to mentalizing and theory of mind (63, 64). Because complex social behaviors are challenging to study directly, we sought tasks that incorporate social and strategic elements as a proxy. One effective approach to probing these deficits in both humans and animal models is through competitive and cooperative games (42, 65, 66). Second, we aimed to use a task that could be implemented in head-fixed mice, allowing us to perform subcellular-resolution imaging of dendritic signals during behavior. For instance, while attentional set-shifting tasks are well established for assessing cognitive flexibility and have been successfully used in ASD mouse models (67), most implementations involve freely moving mice using food bowls, operant nose pokes, or touchscreens (but see ref. 68, which may be a future direction). These considerations led us to test the *Scn2a* mouse model using matching pennies, which is a classic competitive game paradigm. This approach is relatively untested in rodents, but builds on more extensive previous human studies that linked autism-related traits to performance in strategic games such as the stag-hunt (69), repeated rock-paper-scissors (70), and the dictator game (71). Interestingly, some studies suggest that individuals with ASD may not always have deficits but may instead show enhanced rationality and even outperform controls in certain game contexts (72), highlighting the utility of this approach and nuanced nature of decision-making deficits in autism.

In this study, we observed a subtle but statistically significant behavioral deficit for the *Scn2a*$^{+/-}$ mice. There are several reasons why the detected effect was subtle. First, there is individual variability across animals. We tried to minimize variability by carefully standardizing the training environment, however there is still variation in switch rate across individuals of the same genotype. Second, these mice were overtrained. Animals were shaped by first learning matching pennies, where they played repeatedly for tens of thousands of trials against a computer opponent employing the predictive strategy. Once they became proficient, we tested the animals against a computer opponent with changing strategies. Third, likely the strongest factor, computer changed its strategy unbeknownst to the animal. Our analysis was based on dividing trials into blocks based on the computer's strategy, but the mouse needed time to adapt, thus would still play initially in a new block as if it was playing against the old opponent. For future studies, a more powerful way to assess changes in the mouse's behavior would be to divide trials into blocks based on the mouse's latent strategy.

During behavior, reward- and strategy-related signals were diminished in frontal cortical IT neurons of *Scn2a*$^{+/-}$ animals. Prior studies have shown that causally silencing neural activity in the frontal cortical region can impair behavioral adjustments (38, 73), therefore our observed loss of task-related signals may underpin the cognitive rigidity. Notably, our results match a prior study identifying reward-related signals in the dendrites of IT, but not PT, pyramidal neurons in the somatosensory cortex in behaving mice (25). Unexpectedly, we observed an aberrant gain of task-selective signals in the dendrites of PT neurons after the partial loss of *Scn2a*, suggesting that the relevant synaptic inputs not be fully lost, but rather maladaptively wired to alter their processing in the medial frontal cortex. Given that frontal cortical PT and IT neurons underpin distinct aspects of motor and decision-related behaviors (74, 75), the cell-type specific deficits provide insights into the circuit mechanisms in ASD. A limitation of this study is that although we observed altered dendritic signaling, the findings do not establish whether these perturbations are the causal basis of the inflexible decision-making.

Despite the strong causal link from *SCN2A* to ASD, prior studies of the heterozygous *Scn2a*$^{+/-}$ mice reported only mild behavioral changes. For adult animals, there was no notable change in many behavioral assays designed to test locomotion, anxiety, social interactions, and memory (15, 76). There were some phenotypes for *Scn2a*$^{+/-}$ mice, such as decreased ultrasonic vocalization (76), novelty-induced hyperactivity (77), enhanced social interaction (78), and elevated long-term fear memory (77, 78). Phenotypes such as increased responses to lights-on stimuli, daytime hypoactivity, and night-time hyperactivity have also been described in zebrafish models with mutations in the related *Scn1lab* (79). There have been reports of spatial learning deficits in *Scn2a*-haploinsufficient mice (80, 81). A particularly promising trait for translational research is impaired vestibulo-ocular reflex, which is cerebellum-dependent and can be observed in both humans and rodents (82). However, these behavioral phenotypes are difficult to relate to the intellectual deficits observed in humans (12–14). In this study, building on the classic matching pennies game, we developed a task that incentivizes cognitive flexibility.

Testing a large cohort of *Scn2a*$^{+/-}$ mice and *Scn2a*$^{+/+}$ littermate controls, we demonstrated that control animals could adjust bidirectionally to the shifting behavioral strategies, but mice with *Scn2a* haploinsufficiency failed to adapt. We believe our findings have translational significance, because the same competitive or cooperative game can be tested on animal models and individuals with ASD. In fact, one recent study reported a similar variant of matching pennies, where they programmed computer opponents to play with either a cooperative or competitive strategy and evaluated how human participants would adapt (83). We expect cross-species tasks will facilitate the translation of treatments from animal models to humans.

Understanding how ASD risk genes affect dendritic function is crucial because dendrites play a central role in how neurons receive, integrate, and process information. Here, our data provide evidence that the heterozygous loss of the high-confidence risk gene *Scn2a* reduces dendritic coupling in the medial frontal cortex and impairs flexible decision-making. By linking the risk gene to dendritic alterations in vivo, our results provide mechanistic insights into cortical circuit deficits associated with ASD. Deeper knowledge of the neural basis underlying the cognitive symptoms observed in ASD will advance diagnostic and treatment strategies for the disorder.

Methods

Scn2a$^{+/-}$ mice were originally generated via homologous recombination (84) and sourced from the University of California San Francisco. C57BL/6J (Stock #000664). *Fezf2-2A-CreER* (B6;129S4-*Fezf2*$^{tm1.1(cre/ERT2)Zjh}$/J, Stock #036296) and *PlexinD1-2A-CreER1* (B6;129S4-*Plxnd1*$^{tm1.1(cre/ERT2)Zjh}$/J, Stock #036296) mice (2) were purchased from Jackson Laboratory. Animal procedures were approved by the Institutional Animal Care and Use Committees at Yale University and Cornell University. Dendritic calcium signals were acquired using a two-photon microscope (MOM, Sutter Instrument) equipped with an electrically tunable lens (EL-3-10, Optotune). Head-fixed mice were trained to play matching pennies against a computer opponent, using a custom behavioral setup controlled by the scripting language in the Presentation software. In-depth descriptions of animals, surgical procedures, behavioral setup and training, two-photon microscopy, analyses of behavioral and imaging data, and statistical methods can be found in *SI Appendix*.

Data, Materials, and Software Availability. Data and code associated with the study are available at https://github.com/Kwan-Lab/wu2025 (85). Designs for the headplate and behavioral setup used to train head-fixed mice are available at https://github.com/Kwan-Lab/behavioral-rigs (86).

ACKNOWLEDGMENTS. This work was supported by a Simons Foundation Autism Research Initiative Pilot Award (A.C.K.). Additional support was provided by NIH U01NS128660 (A.C.K.), China Scholarship Council-Yale World Scholars Fellowship (H.W.), Cornell Engineering Learning Initiatives (J.I.), NIH training grants T32GM007205 (N.K.S.), NIH fellowship F30MH129085 (N.K.S.), and NIH instrumentation grant S10OD032251 (Cornell Biotechnology Resource Center Imaging Facility).

Author affiliations: [a]Meinig School of Biomedical Engineering, Cornell University, Ithaca, NY 14853; [b]Interdepartmental Neuroscience Program, Yale University School of Medicine, New Haven, CT 06511; [c]Medical Scientist Training Program, Yale University School of Medicine, New Haven, CT 06511; [d]Center for Integrative Neuroscience, Department of Neurology, University of California, San Francisco, CA 94158; and [e]Department of Psychiatry, Weill Cornell Medicine, New York, NY 10065

1. S. De Rubeis *et al.*, Synaptic, transcriptional and chromatin genes disrupted in autism. *Nature* **515**, 209–215 (2014).
2. S. J. Sanders *et al.*, De novo mutations revealed by whole-exome sequencing are strongly associated with autism. *Nature* **485**, 237–241 (2012).
3. F. K. Satterstrom *et al.*, Large-scale exome sequencing study implicates both developmental and functional changes in the neurobiology of autism. *Cell* **180**, 568–584.e523 (2020).
4. A. J. Willsey *et al.*, Coexpression networks implicate human midfetal deep cortical projection neurons in the pathogenesis of autism. *Cell* **155**, 997–1007 (2013).
5. S. B. Nelson, V. Valakh, Excitatory/inhibitory balance and circuit homeostasis in autism spectrum disorders. *Neuron* **87**, 684–698 (2015).
6. A. D. Nelson, K. J. Bender, Dendritic integration dysfunction in neurodevelopmental disorders. *Dev. Neurosci.* **43**, 201–221 (2021).
7. M. T. Lazaro *et al.*, Reduced prefrontal synaptic connectivity and disturbed oscillatory population dynamics in the CNTNAP2 model of autism. *Cell Rep.* **27**, 2567–2578.e66 (2019).
8. X. Wang *et al.*, Synaptic dysfunction and abnormal behaviors in mice lacking major isoforms of Shank3. *Hum. Mol. Genet.* **20**, 3093–3108 (2011).
9. F. Ali *et al.*, Inhibitory regulation of calcium transients in prefrontal dendritic spines is compromised by a nonsense Shank3 mutation. *Mol. Psychiatry* **26**, 1945–1966 (2021).
10. K. O. Lai, N. Y. Ip, Structural plasticity of dendritic spines: The underlying mechanisms and its dysregulation in brain disorders. *Biochim. Biophys. Acta* **1832**, 2257–2263 (2013).
11. M. Phillips, L. Pozzo-Miller, Dendritic spine dysgenesis in autism related disorders. *Neurosci. Lett.* **601**, 30–40 (2015).
12. S. J. Sanders *et al.*, Progress in understanding and treating SCN2A-mediated disorders. *Trends Neurosci.* **41**, 442–456 (2018).
13. A. Begemann *et al.*, Further corroboration of distinct functional features in SCN2A variants causing intellectual disability or epileptic phenotypes. *Mol. Med.* **25**, 6 (2019).
14. R. Ben-Shalom *et al.*, Opposing effects on NaV1.2 function underlie differences between SCN2A variants observed in individuals with autism spectrum disorder or infantile seizures. *Biol. Psychiatry* **82**, 224–232 (2017).
15. P. W. E. Spratt *et al.*, The autism-associated gene Scn2a contributes to dendritic excitability and synaptic function in the prefrontal cortex. *Neuron* **103**, 673–685.e675 (2019).
16. A. D. Nelson *et al.*, Physical and functional convergence of the autism risk genes Scn2a and Ank2 in neocortical pyramidal cell dendrites. *Neuron* **112**, 1133–1149.e36 (2024).
17. T. W. Chen *et al.*, Ultrasensitive fluorescent proteins for imaging neuronal activity. *Nature* **499**, 295–300 (2013).
18. H. Jia, N. L. Rochefort, X. Chen, A. Konnerth, Dendritic organization of sensory input to cortical neurons in vivo. *Nature* **464**, 1307–1312 (2010).
19. D. E. Wilson, D. E. Whitney, B. Scholl, D. Fitzpatrick, Orientation selectivity and the functional clustering of synaptic inputs in primary visual cortex. *Nat. Neurosci.* **19**, 1003–1009 (2016).
20. Y. Otor *et al.*, Dynamic compartmental computations in tuft dendrites of layer 5 neurons during motor behavior. *Science* **376**, 267–275 (2022).
21. J. K. O'Hare *et al.*, Compartment-specific tuning of dendritic feature selectivity by intracellular Ca(2+) release. *Science* **375**, eabm1670 (2022).
22. A. Kerlin *et al.*, Functional clustering of dendritic activity during decision-making. *eLife* **8**, e46966 (2019).
23. C. O. Lacefield, E. A. Pnevmatikakis, L. Paninski, R. M. Bruno, Reinforcement learning recruits somata and apical dendrites across layers of primary sensory cortex. *Cell Rep.* **26**, 2000–2008.e02 (2019).
24. N. L. Xu *et al.*, Nonlinear dendritic integration of sensory and motor input during an active sensing task. *Nature* **492**, 247–251 (2012).
25. N. Takahashi *et al.*, Active dendritic currents gate descending cortical outputs in perception. *Nat. Neurosci.* **23**, 1277–1285 (2020).
26. N. Takahashi, T. G. Oertner, P. Hegemann, M. E. Larkum, Active cortical dendrites modulate perception. *Science* **354**, 1587–1590 (2016).
27. L. Beaulieu-Laroche, E. H. S. Toloza, N. J. Brown, M. T. Harnett, Widespread and highly correlated somato-dendritic activity in cortical layer 5 neurons. *Neuron* **103**, 235–241.e234 (2019).
28. M. E. Sheffield, D. A. Dombeck, Calcium transient prevalence across the dendritic arbour predicts place field properties. *Nature* **517**, 200–204 (2015).
29. A. Baker *et al.*, Specialized subpopulations of deep-layer pyramidal neurons in the neocortex: Bridging cellular properties to functional consequences. *J. Neurosci.* **38**, 5441–5455 (2018).
30. P. G. Anastasiades, A. G. Carter, Circuit organization of the rodent medial prefrontal cortex. *Trends Neurosci.* **44**, 550–563 (2021).
31. L. Gao *et al.*, Single-neuron projectome of mouse prefrontal cortex. *Nat. Neurosci.* **25**, 515–529 (2022).
32. G. M. Shepherd, Corticostriatal connectivity and its role in disease. *Nat. Rev. Neurosci.* **14**, 278–291 (2013).
33. L. X. Shao *et al.*, Psilocybin's lasting action requires pyramidal cell types and 5-HT(2A) receptors. *Nature* **642**, 411–420 (2025).
34. G. Marcassa *et al.*, Synaptic signatures and disease vulnerabilities of layer 5 pyramidal neurons. *Nat. Commun.* **16**, 228 (2025).
35. B. F. Grewe, F. F. Voigt, M. van't Hoff, F. Helmchen, Fast two-layer two-photon imaging of neuronal cell populations using an electrically tunable lens. *Biomed. Opt. Express* **2**, 2035–2046 (2011).
36. F. Ali, A. C. Kwan, Interpreting in vivo calcium signals from neuronal cell bodies, axons, and dendrites: A review. *Neurophotonics* **7**, 011402 (2020).
37. J. Friedrich, P. Zhou, L. Paninski, Fast online deconvolution of calcium imaging data. *PLoS Comput. Biol.* **13**, e1005423 (2017).
38. M. J. Siniscalchi, V. Phoumthipphavong, F. Ali, M. Lozano, A. C. Kwan, Fast and slow transitions in frontal ensemble activity during flexible sensorimotor behavior. *Nat. Neurosci.* **19**, 1234–1242 (2016).
39. S. Schamiloglu, H. Wu, M. Zhou, A. C. Kwan, K. J. Bender, Dynamic foraging behavior performance is not affected by Scn2a haploinsufficiency. *eNeuro* **10**, ENEURO.0367-23.2023 (2023).
40. H. Wang, H. K. Ortega, H. Atilgan, C. E. Murphy, A. C. Kwan, Pupil correlates of decision variables in mice playing a competitive mixed-strategy game. *eNeuro* **9**, ENEURO.0457-21.2022 (2022).
41. H. Wang *et al.*, Frontal noradrenergic and cholinergic transients exhibit distinct spatiotemporal dynamics during competitive decision-making. *Sci. Adv.* **11**, eadr9916 (2025).
42. C. Camerer, *Behavioral Game Theory: Experiments in Strategic Interaction* (Princeton University Press, 2003).
43. C. E. Murphy, H. Wang, H. K. Ortega, A. C. Kwan, H. Atilgan, Change point estimation by the mouse medial frontal cortex during probabilistic reward learning. *eLife*, 10.7554/eLife.103001.1.sa4 (2024).
44. M. Ito, K. Doya, Parallel representation of value-based and finite state-based strategies in the ventral and dorsal striatum. *PLoS Comput. Biol.* **11**, e1004540 (2015).

45. D. G. Tervo *et al.*, Behavioral variability through stochastic choice and its gating by anterior cingulate cortex. *Cell* **159**, 21–32 (2014).
46. D. Lee, M. L. Conroy, B. P. McGreevy, D. J. Barraclough, Reinforcement learning and decision making in monkeys during a competitive game. *Brain Res. Cogn. Brain Res.* **22**, 45–58 (2004).
47. K. S. Matho *et al.*, Genetic dissection of the glutamatergic neuron system in cerebral cortex. *Nature* **598**, 182–187 (2021).
48. H. Seo, D. Lee, Temporal filtering of reward signals in the dorsal anterior cingulate cortex during a mixed-strategy game. *J. Neurosci.* **27**, 8366–8377 (2007).
49. J. H. Sul, H. Kim, N. Huh, D. Lee, M. W. Jung, Distinct roles of rodent orbitofrontal and medial prefrontal cortex in decision making. *Neuron* **66**, 449–460 (2010).
50. M. J. Siniscalchi, H. Wang, A. C. Kwan, Enhanced population coding for rewarded choices in the medial frontal cortex of the mouse. *Cereb. Cortex.* **29**, 4090–4106 (2019).
51. B. A. Bari *et al.*, Stable representations of decision variables for flexible behavior. *Neuron* **103**, 922–933.e927 (2019).
52. R. Hattori, B. Danskin, Z. Babic, N. Mlynaryk, T. Komiyama, Area-specificity and plasticity of history-dependent value coding during learning. *Cell* **177**, 1858–1872.e15 (2019).
53. S. Musall, M. T. Kaufman, A. L. Juavinett, S. Gluf, A. K. Churchland, Single-trial neural dynamics are dominated by richly varied movements. *Nat. Neurosci.* **22**, 1677–1686 (2019).
54. C. Stringer *et al.*, Spontaneous behaviors drive multidimensional, brainwide activity. *Science* **364**, 255 (2019).
55. M. Yun, E. Kim, M. W. Jung, Enhanced fear limits behavioral flexibility in Shank2-deficient mice. *Mol. Autism* **13**, 40 (2022).
56. F. Helmchen, K. Svoboda, W. Denk, D. W. Tank, In vivo dendritic calcium dynamics in deep-layer cortical pyramidal neurons. *Nat. Neurosci.* **2**, 989–996 (1999).
57. U. Marti Mengual *et al.*, Efficient low-pass dendro-somatic coupling in the apical dendrite of layer 5 pyramidal neurons in the anterior cingulate cortex. *J. Neurosci.* **40**, 8799–8815 (2020).
58. J. Waters, F. Helmchen, Boosting of action potential backpropagation by neocortical network activity in vivo. *J. Neurosci.* **24**, 11127–11136 (2004).
59. M. Murayama, M. E. Larkum, Enhanced dendritic activity in awake rats. *Proc. Natl. Acad. Sci. U.S.A.* **106**, 20482–20486 (2009).
60. V. Francioni, Z. Padamsey, N. L. Rochefort, High and asymmetric somato-dendritic coupling of V1 layer 5 neurons independent of visual stimulation and locomotion. *Elife* **8**, e49145 (2019).
61. P. W. E. Spratt *et al.*, Paradoxical hyperexcitability from Na(V)1.2 sodium channel loss in neocortical pyramidal cells. *Cell Rep.* **36**, 109483 (2021).
62. J. Zhang *et al.*, Severe deficiency of the voltage-gated sodium channel Na(V)1.2 elevates neuronal excitability in adult mice. *Cell Rep.* **36**, 109495 (2021).
63. S. Baron-Cohen, M. K. Belmonte, Autism: A window onto the development of the social and the analytic brain. *Annu. Rev. Neurosci.* **28**, 109–126 (2005).
64. U. Frith, F. Happe, Autism spectrum disorder. *Curr. Biol.* **15**, R786–R790 (2005).
65. D. Lee, Game theory and neural basis of social decision making. *Nat. Neurosci.* **11**, 404–409 (2008).
66. H. Wang, A. C. Kwan, Competitive and cooperative games for probing the neural basis of social decision-making in animals. *Neurosci. Biobehav. Rev.* **149**, 105158 (2023).
67. M. M. Cunniff, E. Markenscoff-Papadimitriou, J. Ostrowski, J. L. R. Rubenstein, V. S. Sohal, Altered hippocampal–prefrontal communication during anxiety-related avoidance in mice deficient for the autism-associated gene Pogz. *eLife* **9**, e54835 (2020).
68. T. Spellman, M. Svei, J. Kaminsky, G. Manzano-Nieves, C. Liston, Prefrontal deep projection neurons enable cognitive flexibility via persistent feedback monitoring. *Cell* **184**, 2750–2766. e17 (2021).
69. W. Yoshida *et al.*, Cooperation and heterogeneity of the autistic mind. *J. Neurosci.* **30**, 8815–8818 (2010).
70. K. Arai, S. Jacob, A. S. Widge, A. Yousefi, Deviation from Nash mixed equilibrium in repeated rock-scissors-paper reflect individual traits. *Sci. Rep.* **15**, 14955 (2025).
71. K. Izuma, K. Matsumoto, C. F. Camerer, R. Adolphs, Insensitivity to social reputation in autism. *Proc. Natl. Acad. Sci. U.S.A.* **108**, 17302–17307 (2011).
72. L. Rozenkrantz, A. M. D'Mello, J. D. E. Gabrieli, Enhanced rationality in autism spectrum disorder. *Trends Cogn. Sci.* **25**, 685–696 (2021).
73. D. C. Schreiner, C. Cazares, R. Renteria, C. M. Gremel, Information normally considered task-irrelevant drives decision-making and affects premotor circuit recruitment. *Nat. Commun.* **13**, 2134 (2022).
74. N. Li, T. W. Chen, Z. V. Guo, C. R. Gerfen, K. Svoboda, A motor cortex circuit for motor planning and movement. *Nature* **519**, 51–56 (2015).
75. S. Musall *et al.*, Pyramidal cell types drive functionally distinct cortical activity patterns during decision-making. *Nat. Neurosci.* **26**, 495–505 (2023).
76. I. Lena, M. Mantegazza, Na(V)1.2 haploinsufficiency in Scn2a knock-out mice causes an autistic-like phenotype attenuated with age. *Sci. Rep.* **9**, 12886 (2019).
77. T. Tatsukawa *et al.*, Scn2a haploinsufficient mice display a spectrum of phenotypes affecting anxiety, sociability, memory flexibility and ampakine CX516 rescues their hyperactivity. *Mol. Autism* **10**, 15 (2019).
78. W. Shin *et al.*, Scn2a haploinsufficiency in mice suppresses hippocampal neuronal excitability, excitatory synaptic drive, and long-term potentiation, and spatial learning and memory. *Front. Mol. Neurosci.* **12**, 145 (2019).
79. H. Weinschutz Mendes *et al.*, High-throughput functional analysis of autism genes in zebrafish identifies convergence in dopaminergic and neuroimmune pathways. *Cell Rep.* **42**, 112243 (2023).
80. D. B. Kastner, G. Williams, C. Holobetz, J. P. Romano, P. Dayan, The choice-wide behavioral association study: Data-driven identification of interpretable behavioral components. bioRxiv [Preprint] (2024). https://doi.org/10.1101/2024.02.26.582115 (Accessed 25 April 2024).
81. S. J. Middleton *et al.*, Altered hippocampal replay is associated with memory impairment in mice heterozygous for the Scn2a gene. *Nat. Neurosci.* **21**, 996–1003 (2018).
82. C. Wang *et al.*, Impaired cerebellar plasticity hypersensitizes sensory reflexes in SCN2A-associated ASD. *Neuron* **112**, 1444–1455.e45 (2024).
83. R. Philippe *et al.*, Neurocomputational mechanisms involved in adaptation to fluctuating intentions of others. *Nat. Commun.* **15**, 3189 (2024).
84. R. Planells-Cases *et al.*, Neuronal death and perinatal lethality in voltage-gated sodium channel alpha(II)-deficient mice. *Biophys. J.* **78**, 2878–2891 (2000).
85. H. Wu *et al.*, Autism-associated Scn2a haploinsufficiency disrupts in vivo dendritic signaling and impairs flexible decision-making. GitHub. https://github.com/Kwan-Lab/wu2025. Deposited 13 August 2025.
86. A. Kwan *et al.*, Behavioral rigs. GitHub. https://github.com/Kwan-Lab/behavioral-rigs. Deposited 6 June 2022.